

Improved light extraction in the bioluminescent lantern of a *Photuris* firefly (Lampyridae)

Annick Bay,¹ Peter Cloetens,² Heikki Suhonen,² and Jean Pol Vigneron¹

¹*Research Center in Physics of Matter and Radiation (PMR), Department of Physics, University of Namur (FUNDP), 61 rue de Bruxelles, B-5000 Namur, Belgium**

²*X-ray Imaging Group, European Synchrotron Research Facility (ESRF), BP 220, 38043 Grenoble cedex, France*

A common problem of light sources emitting from an homogeneous high-refractive index medium into air is the loss of photons by total internal reflection. Bioluminescent organisms, as well as artificial devices, have to face this problem. It is expected that life, with its mechanisms for evolution, would have selected appropriate optical structures to get around this problem, at least partially. The morphology of the lantern of a specific firefly in the genus *Photuris* has been examined. The optical properties of the different parts of this lantern have been modelled, in order to determine their positive or adverse effect with regard to the global light extraction. We conclude that the most efficient pieces of the lantern structure are the misfit of the external scales (which produce abrupt roughness in air) and the lowering of the refractive index at the level of the cluster of photocytes, where the bioluminescent production takes place.

Keywords: Physiological optics, Luminescence, Diffusion, Light-emitting polymers.

I. INTRODUCTION

Most living organisms - including ourselves - use light as a primary source of energy and as an information carrier for communication. Since the emergence of vision, light has kept delivering signals, processed into knowledge and exploited at the behavioral level. Vision and light flux management have turned into an essential function for most highly evolved animals. Insects, birds, fishes, and many other living organisms use spectrally filtered sun light for making themselves conspicuous to their mates, warn predators of toxicity, signal territory occupancy, hide from the view of preys or predators and much more.

At dusk, when the sun disappears from view, and when the direct sun illumination vanishes, the importance of light does not weaken. Many organisms have adapted to moonlight intensities and keep a clear vision at night. Also, quite a few animals produce their own light by bioluminescence and use it for communication in the dark. There are two great categories of bioluminescent species: one in deep waters, the other terrestrial. Bioluminescent animals from the deep are usually emitting blue and get the help of symbiotic luminescent bacteria [1] to produce their light. In such an association, a bacteria such as those in the genus *Photobacterium* takes care of the chemistry needed to produce photons, in response to the host's needs. Unicellular algae *Pyrodinium bahamense* also produce light, especially in disturbed waters. The "Phosphorescent Bay" of Vieques, Porto Rico, is a well-known place – among many others – where these dinoflagellates can easily be observed producing a halo of blue light following boat tracks.

Some terrestrial animals such as insects also produce their own light. The colors are most often in the yellow-green range, but orange-red is also frequent. Perhaps the best known are fireflies (see Fig. 1), in the family Lampyridae, for which all phases, eggs, larvae, pupae and adults, males and females, can produce light. Eggs and larvae produce a continuous light emission. It is assumed that this illumination is a warning signal against the predators, as in other steady bioluminescent insects such as click-beetles (Elaterridae: *Pyrophorus*), which start emitting a strong continuous signal when disturbed or otherwise threaten. In some species, male and female adult fireflies lanterns are more complex [2], with the capability of flashing the bioluminescent emission. Each species has its own specific light pulse pattern, which acts as a communication signature: the female is usually at rest at the edge of the forest while males are flying around, sending and receiving signals. The females respond to "their" males [3] to reveal their location, and reproduction is initiated. A perversion of this behavior is known, as the females of the firefly *Photuris versicolor* is able to mimic the light flash pattern of some *Photinus* females in order to attract their males and prey on them [4], absorbing nutrients and more [5]. The chemical reaction that creates photons from the energy stored in adenosine triphosphate has been described as the oxidation of a substrate of luciferine catalyzed by the enzymatic luciferase. Different types of luciferine-luciferase pairs have been described, leading to different colors. What is not so

*Electronic address: annick.bay@fundp.ac.be



FIG. 1: The *Photuris sp.* firefly, collected in the Darien forest, Republic of Panama, whose lantern is investigated in the present work.

well understood is the way the bioluminescence can be switched on and off to produce flashes that, sometimes, can be short (pulse duration under a second) and undergo amazingly fast rises and falls.

Another problem – which has been neglected up to now, except maybe for a preliminary report of part of the present work in a conference abstract [6] – is the optical origin of the *external* efficiency of the firefly lanterns. When a source emits from inside a high refractive index medium, the emitted light that reaches the surface will not always be able to escape into the air, because of the total reflection at large incidence angles. The external efficiency of all electroluminescent devices made from semiconductors [7] is affected by this effect, and this is especially true for the recently developed large-size organic light-emitting diodes [8, 9]. The firefly lantern is no exception and it is interesting to parallel the decades of semi-conductor diodes structural optimized engineering with some hundred million years of blind natural selection in these living organisms.

The present work considers the photonic structure of the various parts of the insect’s lantern in order to recognize, on the ground of computer simulations, those who plausibly contribute best to the improvement of the light extraction.

We will carry out this work in five steps : (1) [section II] a reference system is first defined; (2) the results of morphology investigations is reported; (3) computer simulations of the optical behavior of each individual recognized substructural lantern element and conclusions on the positive or adverse effect on light extraction are presented; (4) a global model, that takes into account the set of relevant substructures, will be considered in order to provide some theoretical estimate of the external efficiency; (5) finally, we show how these calculated estimates get support from direct observations.

II. LIGHT EXTRACTION FROM AN HOMOGENEOUS MEDIUM TERMINATED BY A PLANAR SURFACE

We do not know how fireflies looked like some hundred million years ago, so it is difficult to use the ancestors’ extraction organs as a reference to which compare the lanterns that are around today, in nature. Our reference, in order to discuss possible improvements, will be based on an idealized physical model system consisting of an homogeneous medium in contact with air at a planar surface. We will set an isotropic point light source at some macroscopic distance under a perfect flat surface and evaluate the fraction of the emitted light intensity that effectively crosses the surface to be released in the open air (in the emergence medium hemisphere). This fraction will represent the external efficiency reduction factor. All subsequent calculations, when the structured parts of the firefly lantern will be included, will be treated in exactly the same way.

Shown in Fig. 2, a point source emits uniformly at a depth z in a medium of refractive index n_i , limited by a plane surface. It illuminates this surface in a non-uniform way. If a sphere with unit radius is drawn, centered on the source, the total power emitted through its upper hemisphere is $P_0/2$, where P_0 is the total radiant energy emitted each second by the source. Assuming that there is no absorption between depth z and the surface, the fraction of this power sent out in a solid angle $d\Omega$, under the incidence angle θ_i is then

$$\frac{d\Omega}{2\pi}(P_0/2) = \frac{d\vec{s} \cdot \vec{u}}{2\pi\rho^2}(P_0/2) = (P_0/2) \frac{ds \cos \theta_i}{2\pi\rho^2} \quad (1)$$

where: $d\vec{s}$ is the element of horizontal plane surface intercepted by the solid angle $d\Omega$; \vec{u} is a unit vector in the light propagation direction with incidence angle θ_i ; ρ is the distance between the source and the surface element.

The horizontal surface element can be expressed in polar coordinates r and ϕ , $ds = r dr d\phi$ to give (with $r = z \tan \theta_i$)

$$\frac{d\Omega}{2\pi}(P_0/2) = \frac{(P_0/2)}{2\pi} \sin \theta_i d\theta_i d\phi \quad (2)$$

The total power incident on the plane surface can be obtained by integrating this contribution over all surface elements, which leads us to the expression

$$P_i = (P_0/2) \int_0^{\frac{\pi}{2}} \sin \theta_i d\theta_i \quad (3)$$

This, as expected, turns out to be $P_0/2$. The power transmitted into the outer medium, with a refractive index n_t depends on the transmission coefficient $T(\theta_i)$ of the interface for each incidence θ_i . The total power transmitted can then be obtained as

$$P_t = (P_0/2) \int_0^{\frac{\pi}{2}} T(\theta_i) \sin \theta_i d\theta_i \quad (4)$$

The fraction of the incident energy transmitted in the outer medium is then given by

$$\frac{P_t}{P_i} = \int_0^{\frac{\pi}{2}} T(\theta_i) \sin \theta_i d\theta_i \quad (5)$$

This result is independent of the depth z from which the light is emitted, due to the lack of a naturally defined length scale for an homogeneous material under a flat surface.

The transmission coefficient for a planar interface that separates two dielectric media is given explicitly by Fresnel's formula's. For unpolarized light, we have the average of transverse electric and transverse magnetic transmissions :

$$T(\theta_i) = \frac{1}{2} \left\{ \frac{\sin^2(\theta_i - \theta_t)}{\sin^2(\theta_i + \theta_t)} + \frac{\tan^2(\theta_i - \theta_t)}{\tan^2(\theta_i + \theta_t)} \right\} \quad (6)$$

where the angle of emergence θ_t is obtained from Snell's law of refraction,

$$\sin \theta_t = \frac{n_i}{n_t} \sin \theta_i \quad (7)$$

These expressions can be used in the integral (5) in order to obtain the total transmission, integrated over all incidence angles θ_i . In the reference system we consider, we require $n_i = 1.56$, which is the refractive index found in hard parts of the insect's cuticle [10–12], and $n_t = 1$, the refractive index in air. Since the refractive index of the

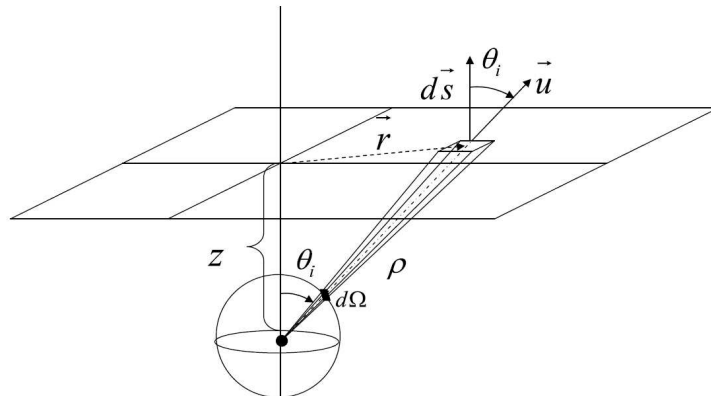


FIG. 2: Geometric data for the integration of the transmitted light over the surface of the reference homogeneous system.

incidence medium is larger than the refractive index of the emergence region, we will have total reflection for incidence angles θ_i larger than the critical angle θ_c given by

$$\sin \theta_c = \frac{n_t}{n_i} \quad (8)$$

The transmission coefficient $T(\theta_i)$ vanishes for $\theta_i > \theta_c$ and the integration (5) needs not be carried out further above this limit.

The integral in (5) can easily be carried out numerically, to any needed accuracy, using a variable-step routine [13]. For the homogeneous medium of refractive index of 1.56, we find a global transmitted fraction of 20%.

This result may seem surprisingly low, especially for a medium with a very moderate refractive index, such as the one considered here. It should be noted that with these refractive indexes, the critical angle for total reflection is 40° , as given by (8), so that none of the incidence angles θ_i between 40° and 90° contribute to the transmission. At small angles, for θ_i near 0° , the geometric factor $\sin \theta_i$ also cuts the transmission efficiency, even if the Fresnel's transmission coefficient is strong there (about 95%).

This 20% transmission will be our reference in the models we will be developing in the next sections. But before coming there, we will describe the structures in which the emitted light has to propagate, from the air down to the photocytes (the light-emitting cells), outside the cuticle surface.

III. MORPHOLOGY OF OPTICAL MEDIA IN THE FIREFLY LANTERN

Morphological studies have been carried out on a *Photuris* firefly. Details on collection of the specimens, the determination of the genus, as well as the sample preparation, used analyzing techniques and simulations tools are given in the section "Materials and Methods" at the end of this paper.

Typical SEM images of these structures are shown in Fig. 3. In order to facilitate the description of the observed features, Fig. 4 summarizes the observations gathered on the structure of the luminescent abdominal segments, on

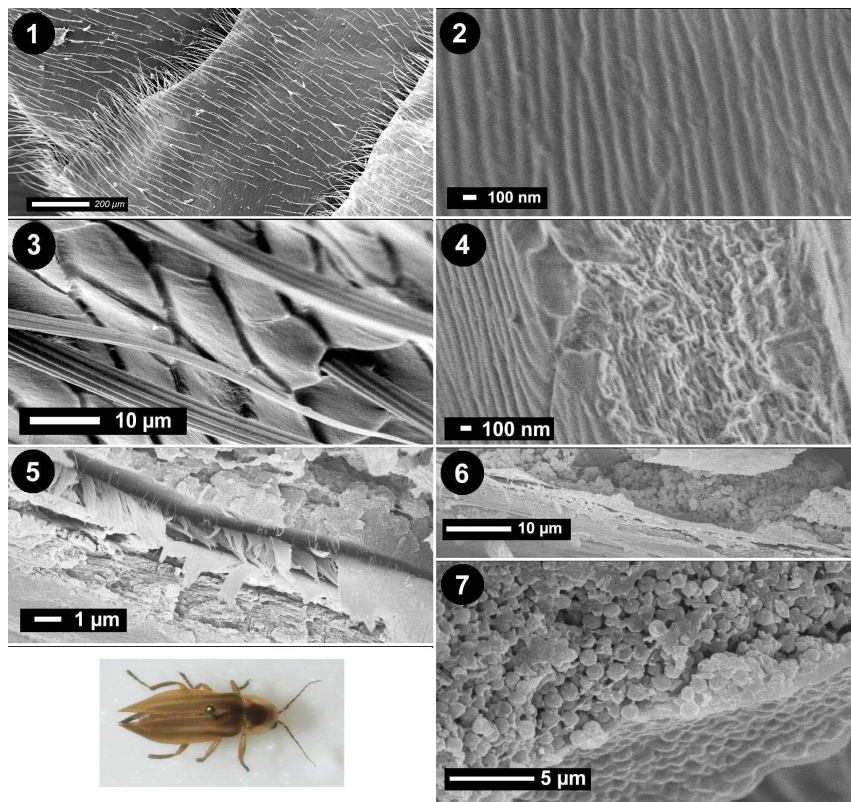


FIG. 3: Observed structures crossed by the emitted light in the lantern of the firefly. (1) Setae; (2) ribs separated by 250 nm; (3) misfit scales, $10 \mu\text{m}$ long and $3 \mu\text{m}$ high; (4) textured cuticle volume, $2.4 \mu\text{m}$ thick. The insert is a top view of the structure; (5) muscular layer (tentative interpretation), variable thickness; (6) photocytes cluster membrane, 60 nm thick; (7) photocytes layer, containing a high density of spherical peroxisomes.

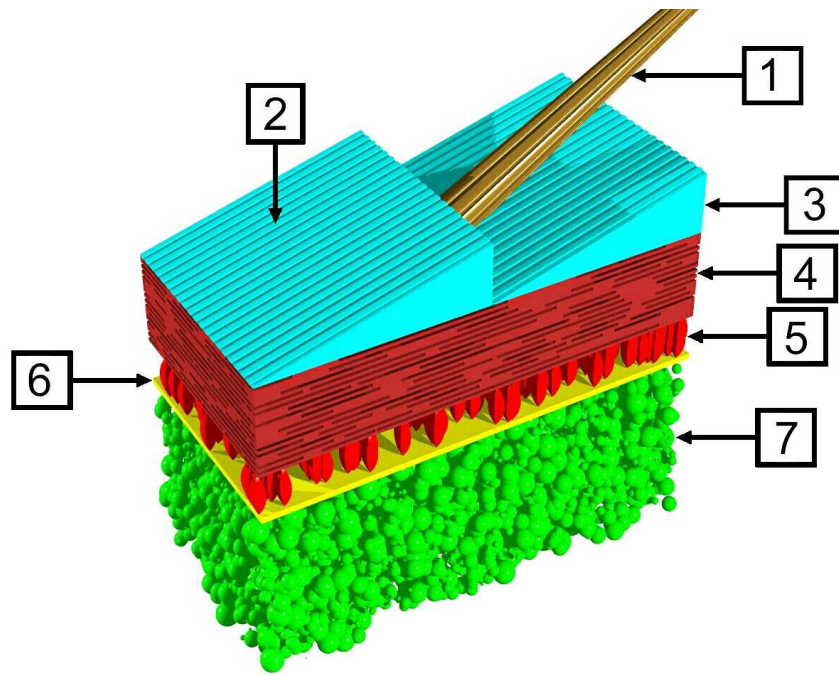


FIG. 4: The various structures to be examined for light extraction improvement. (1) Setae; (2) ribs separated by 250 nm; (3) misfit scales, 10 μm long and 3 μm high; (4) textured cuticle volume, 2.4 μm thick; (5) muscular layer (tentative interpretation), variable thickness; (6) photocytes cluster membrane, 60 nm thick; (7) Photocytes layer, containing spherical peroxisomes.

the ventral side of the insect. Seven photonic sub-structures have been identified, which have a potential impact on the light extraction efficiency.

Substructure (1). The setae found on the cuticle are rigidified by longitudinal ridges, as often in arthropods. These straight, conical projections are likely part of sensitive organs. They can conduct light and scatter it out, but they are not numerous and their cross-section (5 μm in diameter) is small compared to their nearest neighbors' distance (50 μm).

Substructure (2). The cuticle surface is divided into scales – see structure (3), below – and the scales surface show roughness arising from a fine grating of parallel ribs. The ribs are separated by a distance of 250 nm and are typically protruding 100 nm above the scale surface. The cross-section profile of these ribs is very smooth.

Substructure (3). The cuticle of the abdominal segments is composed of scales joined together at their perimeter. However, contrasting many other Coleoptera, the scales do not constitute a flat pavement, but one of the edges (towards the abdominal tip) is slightly protruding. This misfit between scales gives rise to an abrupt running edge which can contribute to light scattering and, through this mechanism, impacts the overall light extraction. The average distance between the protruding edges rows is about 10 μm , long compared to the emitted light wavelength, but surprisingly small, compared to the usual size of Coleoptera scales. The height of the protrusion is variable, but 3 μm is a frequent value.

Substructure (4). Just below the scales, we note a layer, 2.4 μm thick, which makes the bulk of the tegument in the abdominal segment. This layer is a stack of about 30 plates, each 80 nm thick. Each plate is composed of an homogeneous chitin slab, 30 nm thick, bearing a network of parallel rods which act as spacers for the next plate. The spacers corrugation forms a regularly spaced grating with a profile close to that found in the ribs, on the scale surface. The distance between the spacers is of the same order as that of the surface grating, 250 nm. The height of the corrugation associated with these spacers is 50 nm.

Substructure (5). The next inner layer is seen to be essentially empty, except for a large number of fibers which bind to the neighboring layers, (4) and (6). It is difficult to provide data on the thickness of this layer because it is found to be variable over a very wide range. Many different samples provide very different values and it is plausible that this gap between solid layers is tunable by muscular contractions.

The fibers found there may then be some remains of muscles, that can control the geometry of the gap. This interpretation is still very tentative but, if correct, it may be important for the understanding of the production of very fast pulses by the firefly. The very fast “on” and “off” switching of the bioluminescent chemical reaction that produce light pulses is still unexplained because of apparent timing inconsistencies. In particular, the fast admission of

oxygen to start the reaction and the fast injection of an inhibitor to stop it cannot be accounted for by fluid diffusion, considered too slow. A strong pump mechanism would be needed, and this may be provided by the action of muscles that act on the reaction chamber directly, taking its bearing on the mechanically stiff layer (4). Insect muscles can be assumed to be fast and strong enough to produce the fast fluid motion needed to control the emission switch. Further work is in progress to assess the real value of this suggestion, which should, at the moment, be taken with care.

Substructure (6). The gap described in (5) opens on a solid, flexible membrane, 60 nm thick, which separates this “fibrous” gap from the chamber (7) where the bioluminescent reaction takes place.

Substructure (7). The reaction chamber is found below the above layers. It appears to be filled with granular bodies, close to spheres: the peroxisomes. Peroxisomes have been recognized as organelles by the cytologist Christian de Duve in 1969 [14]. One of the main function of these organelles is to eliminate toxic peroxides. They contain a crystalline core and are known to incorporate high quantities of urate oxidase and other enzymes. Figure 4 shows a particularly large quantity of peroxisomes in the layer where the bioluminescence is taking place. These granules, with an average diameter of $0.9 \mu\text{m}$, appear on this SEM image to be densely packed, providing a macroporous disordered structure.

This disordered structure has been confirmed by an X-ray nanotomography experiment conducted at the European Synchrotron Radiation Facility (ESRF) in Grenoble (France) (see “Materials and Methods” section at the end of this paper). This technique does not require the lantern fracturing to observe the volume disorder of the lantern. This presents a huge advantage in comparison to SEM which is a more invasive technique. Three-dimensional data describing the firefly photocyte’s was generated, with about 50 nm pixel size. It is found that the peroxisomes assume a continuous range of diameters, from 0.3 to $1.5 \mu\text{m}$. The disorder is not only a disorder of sphere positions but also a disorder in the size of the spheres. This increased disorder reinforces the argument that the photocyte medium optically behaves as an homogeneous material. The lower refractive index of this averaged medium impacts light extraction by slightly changing the critical angle for total reflection. No directional correlation is found in the spherule arrangement, implying that the peroxisomes distribution avoids both long-range and short-range orders (see Fig. 5(a)). This information suggests that the peroxisomes arrangement cannot drive the emitted light preferentially normal to the cuticle surface as ordered photonic crystals can plausibly do [15]. The multiple scattering of light in this strongly disordered structure is primarily expected to evenly diffuse the emitted light in all directions. This provides support for modeling this isotropic region as a homogeneous medium with an averaged refractive index.

The filling factor of this structure can be estimated to be close to 75%, similar to that of periodic hard-sphere compact structures. Figure 5(b) shows the assembly of spherical granules together with the remains of a fractured tracheole, confirming that the structure is indeed the place where the oxidation reaction takes place: the tracheoles drive oxygen to the porous structure when sustaining the bioluminescence reaction that produces light.

IV. CALCULATION OF LIGHT PROPAGATION IN THE LANTERN SUBSTRUCTURES

We will now reconsider all the substructures revealed by the scanning electron microscopy analysis as described in the previous section and, on the basis of computer simulations, investigate the optical properties of each observed substructure separately in order to discuss their possible contribution to light extraction.

For propagation calculations, we solve Maxwell’s equations, which means that we use a fully vectorial representation of the light waves and we account for multiple scattering at all stages of the calculations. We use transfer-matrix

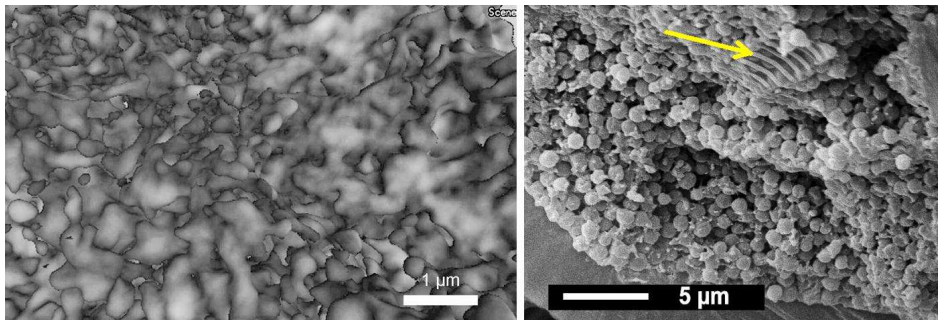


FIG. 5: (a) X-ray nanotomography landscape image, extracted from a three-dimensional representation of the internal structure of a photocyte. These three-dimensional data confirm a disordered and slightly multi-dispersed distribution of the peroxisomes, suggesting an isotropic diffuse light emission. (b) Spherical peroxisomes in the photocytes. Note the remains of a fractured tracheole (arrow) which brings oxygen for the luciferine oxidation.

techniques [16] to calculate transmissions through both one-dimensional and two-dimensional photonic-crystal films (see “Materials and Methods” section).

The light emitted by the firefly is a yellow-green color of narrow spectral range. A wavelength of 560 nm is adequate to represent the color of the flashes and all the simulations in this section will be carried out for this specific wavelength.

The angular distribution of the incident light is kept identical to that defined in the reference model. The different light rays impinging on the surface under different directions are considered incoherent. It should be noted that these rays represent radiation arising from an extended source (the cluster of photocytes) whose different parts emit incoherently.

In the following we use for all relevant substructures diffused intensity diagrams that describes the integrated intensity of the light scattered in the whole emergence hemisphere as a function of the incident polar and incident azimuthal angle (θ and ϕ). These diagrams are important to appreciate the contribution of each substructure to the light scattered out of the medium, especially for incidences in the total reflection conditions of the reference system.

Substructure (1). The cross section of the setae represent less than 1% of the surface offered to light transit so that, even if they are expected to deliver much of the light they carry, their contribution to the external efficiency will be low. They are probably not dense enough to have a strong positive effect on the light extraction. However, they should not show any adverse effect.

Substructure (2). The ribs on the scales form a grating with a period $b = 250$ nm (see Fig. 6(a)). This lattice does produce diffraction, which allows to use some of the light which, otherwise, would have been lost in the total reflection. The structure produces both refraction (transferring light from a medium of refractive index n_i into a medium with refractive index n_t) and diffraction, changing the tangential wave vector component by $m(2\pi/b)$ in the direction normal to the ribs. For light impinging at right angle with the ribs, for instance, the emergence angles θ_t are related to the incidence angle θ_i through the Eq. (9)

$$\sin \theta_t = \frac{n_i}{n_t} \sin \theta_i + m \frac{(\lambda/n_t)}{b} \quad (9)$$

For instance (see Fig. 6(b)), for an angle of incidence $\theta_i = 60^\circ$, well within the total reflection region, the order $m = -1$ produces a transmitted beam which escapes under $\theta_t = -62.7^\circ$ (backscattered). When the azimuthal angle ϕ is changed, the angle of emergence is increased (grazing backscattering) and the diffraction disappears for incidence planes close to parallel to the ribs.

This, however does not inform us on the impact of diffraction on the efficiency of the light extraction. We must calculate the intensity of the transmitted beams ($m = 0$ and $m = -1$) and integrate these on all incidence angles before reaching any conclusion. This has been done with a model where the profile is approximated by a simple sine square function

$$z(y) = h \sin^2 \left(\frac{\pi}{b} y \right) \quad (10)$$

Eqs. (9) and (10) only address relationships between the incident and emergent polar angles and are completely independent of the polarization state of the incident light. They do not provide information about scattering intensities which actually depend on the polarization.

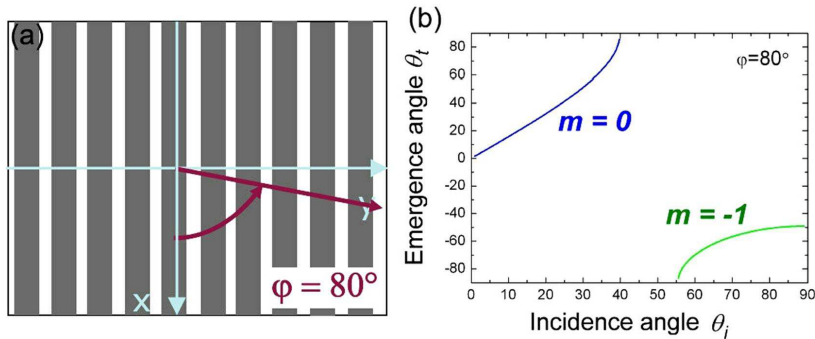


FIG. 6: Diffraction by the 250 nm grating formed by the (a) longitudinal ribs on the surface of the firefly abdominal scales for a fixed incident azimuthal angle $\phi = 80^\circ$. The diagram in (b) results from application of Eq. (9). This shows the existence of diffracted orders ($m=-1$), but does not provide any information about their intensities. These are calculated and reported in Fig. 7.

The distribution of hemispheric intensities as a function of the incident (polar and azimuthal) angles θ_i and φ_i are shown in Fig. 7. Incident azimuthal angles are counted in the x-y plane (see Fig. 6). For symmetry reasons, we account only for the half hemisphere. The polar angle θ is defined from the direction perpendicular to the interface, whereas the azimuthal angle ϕ is defined in the plane of this interface. Azimuthal angles of 90° and 270° correspond to incidences perpendicular to the ripples, whereas an azimuthal angle of 180° corresponds to an incidence parallel to these ripples.

We note that, except for the low diffracted intensities for polar incident angles larger than 40° the hemispheric transmission is very close to that expected from a planar surface. The integration of this distribution gives a total transmission of 20.65% for the TE incident polarization and similar numbers for TM incident polarization (see "Material and Method" section): the corrugation does not improve significantly on the initial 20% transmission of the flat surface. This corrugation is too weak and the grating period is too small to bring any significant change in the light extraction.

Substructure (3). The misfit of scales gives a larger size corrugation, and this gives more opportunities to produce diffracted beams of large order. In calculating the effect of this corrugation, we must ensure that the calculation has converged as a function of the number of diffraction orders included.

The model consists of an array of oblique tiles $10 \mu\text{m}$ long, slanted in such a way that one of their side is protruding $3 \mu\text{m}$ out of the surface. This gives a sharp edge, repeated every $10 \mu\text{m}$, giving a large-step grating. The distribution of the transmitted light, including all diffracted orders, is shown in Fig. 8 as a function of the polar and azimuthal incidence angles. An azimuthal angle of $\phi = 90^\circ$ corresponds to an incidence perpendicular to the sharp edges, $\phi = 180^\circ$ corresponds to an incidence parallel to the protruding edges and $\phi = 270^\circ$ describes an incidence perpendicular to the slope of the edges

The result is quite different from that produced by a short-period grating as the one considered in the substructure (2). The directions, above $\theta_i = 40^\circ$ for which total reflection was expected are now strongly transmitting. The optical phenomenon is actually better described as light scattering on the edges of the tiles, as separated diffraction beams are not perceived.

The origin of this redistribution of light is then qualitatively different from the the mechanism mentioned in the ribs grating (2) above, because of the edges separation ($10 \mu\text{m}$). The integrated transmission also reaches a more interesting value : 29.5% (an average between the results for TE incident polarization, 29.3% and TM, 29.6%, with 32 diffraction orders). The scattering by the scale edges, with the large maintained misfit, improves very significantly the light extraction, adding 47.5% more light out.

The significant increase of light transmission at the protruding edges of the scales is confirmed by the observation of the non-uniform transparency of the cuticle. Figure 9 clearly shows the higher light intensity exiting from the scale's edge, when the cuticle is illuminated from the photocyte location and observed from the outside of the abdomen. In order to obtain this image, an Olympus BX61 optical microscope (objective 60X) was used in transmission mode. The incrustation in Fig. 9 shows an intensity profile across the scale edge, in the image plane. The maximum intensity is obtained on the protruding side of the edge, while a darker fringe develops on the lower side.

Substructure (4). This structure is the repetition, 30 times, of a double layer 80 nm thick, made of 30 nm of solid chitin, and a 50 nm inhomogeneous layer that can be treated with the sine-square model described by Eq. (10). The lateral period of this sine square is $b = 250 \text{ nm}$, as for the surface ribs grating. We have seen already that this period

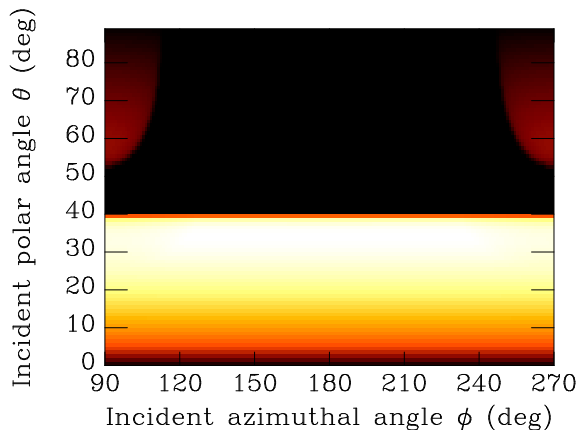


FIG. 7: Hemispheric transmission (logarithmic scale) of a sine-square grating with step $b = 250 \text{ nm}$, as a function of the incidence angles (polar and azimuthal). The geometric factor $\sin \theta_i$ is included. See Eq. (5). The intensities above $\theta_i = 40^\circ$ are diffracted.

provides very few diffracted waves (order $m = -1$). The calculation of the integrated hemispheric transmission can be carried out as before, giving 20.7% as a result. This value, as for the surface ribs corrugation, is not significant and we conclude that the volume corrugation of the cuticle has little (but also, no adverse) effect on the light extraction. The function of this inhomogeneity may be mechanical stiffness.

Substructure (5). The “muscular” layer is difficult to optically characterize, as the contents and thickness range are not precisely known. With a thickness as small as 90 nm, frequent on SEM observation, its effect on the light transmission is weak. It will simply be included later in a more global model before bringing our conclusions from this study.

Substructure (6). This membrane is extremely thin (60 nm on the average) so that its effect on the light transmission is very limited. It will also be included in a more global model below, but we will not consider it separately.

Substructure (7). The optical structure of the reaction chamber, with the accumulation of peroxisomes, is another interesting structure, with no equivalent, to our present knowledge, in other insects. The confinement of the chemical reactants certainly has some influence on the internal quantum yield [17], which depends on the photon density of state, which is highly dependent on the inhomogeneous refractive index distribution. The internal efficiency of the bioluminescent reaction turns out to be close to 88% [18]. The average refractive index found in the chamber is, however lower than that of chitin, because of the presence of the spherical peroxisome : urate, with a refractive index of 1.4, produces a significant lowering of the “incident medium” refractive index (containing the source) and this lowering must lead to a displacement of the critical angle for total reflection. Assuming a regular hexagonal compact assembly of the peroxisome spheres, with a filling factor of 0.74, one can estimate an average refractive index of 1.38, assuming a lower (1.33) refractive index in the small interstitial volume. The critical angle, as given by Eq. (8) turns out to be 46.4° in that case. This supplement of 6° compared to our homogeneous reference opens a new track for light escape and improves the overall external yield.

V. GLOBAL MODEL

We have estimated the gain by considering a more global model, in which all constituents propagating the light are included together: the incident medium is homogeneous, with a refractive index $n_i = 1.38$, separated from a “muscular” gap of 90 nm by a thin membrane (60 nm) with a refractive index 1.56, a $2.4 \mu\text{m}$ thick cuticle layer with an average refractive index of 1.38 and a surface terminated by a triangular profile representing the $10 \mu\text{m}$ scales. The average refractive index of 1.38 was calculated by a procedure similar to that used for averaging the dielectric constant for the coloring structure of the blue beetle *Hoplia coerulea* [19], indeed very similar to the structure found here, except for the layer thicknesses. The ribs and the setae on the surface of the scales, at the outer surface, are neglected because they were shown, above, to only contribute weakly to the light extraction.

The photocytes cluster (incident region) is considered homogeneous, which means that we neglect diffraction by this medium. This is justified by the moderate difference of refractive index between the peroxisome spheres and the fluid interstitial medium, but also because of the isotropic spherules organization.

The transmission for all incidence angles is shown in Fig. 10. Due to multiple scattering, we obtain a rather

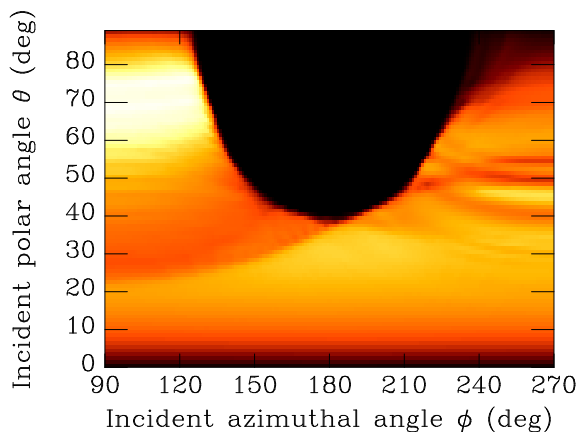


FIG. 8: Hemispheric transmission (logarithmic scale) of a grating with a triangular profile, with step $b = 10 \mu\text{m}$, as a function of the incidence angles (polar and azimuthal). The geometric factor $\sin \theta_i$ is included. See Eq. (5).

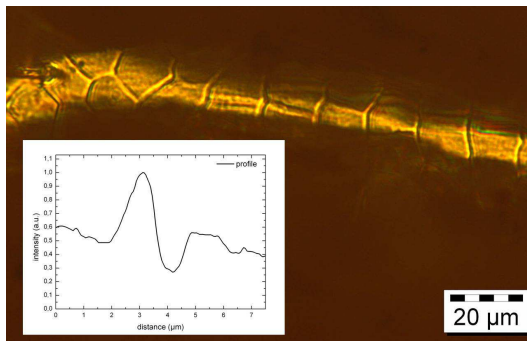


FIG. 9: Light transmission image of the scales covering the surface of one of the firefly’s light-emitting segments, viewed in an optical microscope with illumination set for transmission through the sample. The high-intensity trace concentrated on the edges of the protruding scale adds to the transmitted intensity and favors light extraction. The incrustation shows an intensity profile across the scale edge, in the image plane.

uniform angular distribution of the light, except for $\varphi_i = 0$ or $\varphi_i = 180^\circ$, if θ_i exceeds the critical angle of 46° . These azimuthal angles correspond to light impinging on the surface grating in the “long” direction, where the grating experiences a total translational invariance. In that direction, we recover the flat-surface condition and the concept of a critical angle reappears. We should note that the strictly two-dimensional grating, with one invariant direction, is an approximation. The scales edges are not exactly rectilinear and the scales area is actually limited in two directions.

The integration of the transmission into the full emergence hemispheric solid angle for all incidence angles leads, for this global model, to a transmission of 39.6%, to be compared to the 20% found for the homogeneous medium with a planar surface. This value is for unpolarized light, the average between 37.9% for TE waves and 41.3% for TM waves. The fraction of the enhancement specifically due to the lowering of the incident medium refractive index is of the order of 5%.

VI. SUPPORT FROM DIRECT OPTICAL MEASUREMENT

An experimental check of these theoretical results could be carried out by measuring the hemispheric radiance of the firefly ventral side of the abdomen, while internally illuminating the photocytes. The abdomen of a *Photuris* firefly was separated from the thorax and an optic fiber, connected to a white halogen light source, was introduced along the antero-posterior direction, through the thorax/abdomen section. The radiance ($\text{W}/\text{sr}/\text{m}^2/\text{nm}$) of the ventral side was measured in a solid angle spanning all azimuthal angles and polar angles from 0 to 80° in a ELDIM EZ Contrast XL80MS scatterometer (see “Materials and Methods”), for wavelengths close to the bioluminescent maximum spectrum. The hemispheric radiance due to the scattering of the injected light by the photocyte structure and the extracting structures examined in the present work was calculated from the detailed data by integration over the

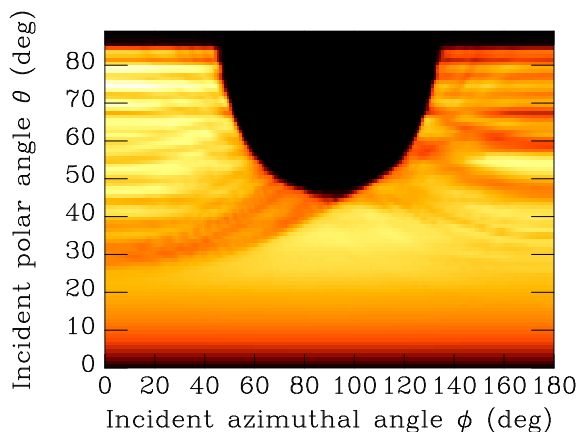


FIG. 10: Hemispheric transmission (logarithmic scale) of the whole structure, as a function of the incidence angles (polar and azimuthal). The geometric factor $\sin \theta_i$ is included. See Eq. (5).

measured solid angle. The result is given by the red curve in Fig. 11. Then, the same experiment was carried out after the surface of the segments were coated with a wetting liquid chosen to match the refractive index 1.56 of chitin. It was expected that the wetting liquid reduced considerably the microscopic corrugation on the firefly abdomen, so that the extracting advantage of these diffusers would be significantly reduced. This is what has been actually observed (see blue curve in Fig. 11). Note that only ratios of these values can be compared to the theoretical prediction, as the reference systems are optically slightly different. The extraction gain, due to the corrugation wiped out by the liquid can be estimated to be above 7% at 560 nm, which means that some improvement of the light extraction is actually observed. In this measurement we consider no change of the refractive index, only the addition (or deletion) of the specific tilted-scale structure. Therefore, the comparison has to be done with the simulations of substructure (3), i.e. to a light extraction gain of 9.5% in comparison to a plane surface (see section IV). The measurement approves the simulation and gives an experimental support. The difference of 2% is acceptable considering that for the measurements, the actual light source is outside of the abdomen and not inside the chitin, like in the simulations. The lantern of the dried specimen contains probably a lot of air spaces, which can influence the path of light.

VII. CONCLUSION

The most effective mechanism found for the light extraction from the lantern of fireflies is the diffuse transmission, produced by the misfit of the scales and the resulting abrupt profile found on the cuticle of the luminous ventral segments. Another, secondary, improvement comes from the lowering of the refractive index at the level of the photocytes, where the bioluminescence chemistry takes place. The other structures found and analyzed do not contribute to a better efficiency but are not detrimental.

These results, however, are only valid for the actual firefly species we have examined. Many other insects produce their own light and, for each of them, a careful analysis of their morphology would be extremely useful. Fireflies and click-beetles, for instance, do not all emit the same wavelength and it would be interesting to know whether some correlation can be found between the emitted wavelength and the optimized structures. With only one example, it is obviously too early to dare any generalization.

The problem of light extraction in fireflies is strongly correlated with many difficulties that must be faced when developing artificial light sources from the solid state. As in many other fields, a biomimetic approach might be helpful when addressing these questions. The lowering refractive index of the active emitting region and the introduction of a specific diffusing roughness on the external surface of the device are reasonable steps to be taken when considering the improvement of solid-state light sources.

Appendix: Materials and Methods

In this section, we briefly introduce experimental techniques and simulation highlights used in the present work. The specimens needed for the present study were all collected in the Darien forest, at the Cana Field Station, in

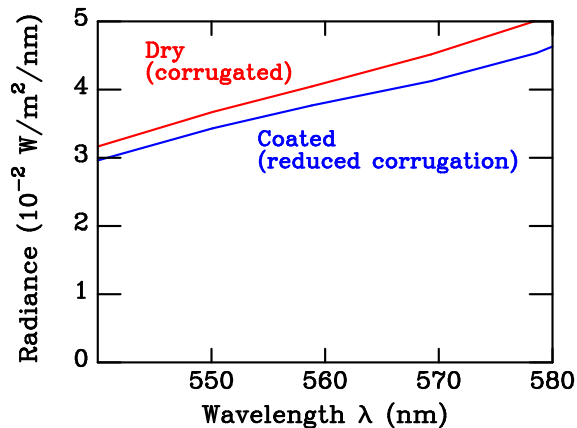


FIG. 11: Hemispheric radiance of the abdomen of a *Photinus* firefly, with (red) and without (blue) its surface corrugation. The suppression of the corrugation, in the latter case, was obtained by coating the ventral part of the abdomen segments with a refractive-index matching liquid.

the back country of the Republic of Panama. The fireflies were found flashing mainly on the grassy air strip which gives access to the station and on bordering trees. The **collection** started near 9 pm, on a clear moonless night, early in May.

A **taxonomic determination** of the collected fireflies was attempted by comparing our specimens with those kept in museums collections. The section of Lampyridae from the Royal Belgian Institute of Natural Sciences in Brussels and of the National Natural History Museum of the Smithsonian Institution (Washington D.C.) were examined and the subfamily – Photurinae – and the genus – *Photuris* (LeConte, 1851) – could be determined. The exact species was doubtful. Close matches, on external traits, included *trilineata*, a species that has been encountered in Panama or close Colombian areas.

The specimens used in this study were examined with **Scanning Electron Microscopy** (SEM). For this investigation, small areas from the ventral side of the abdomen were cut in liquid nitrogen and mounted, cross-section face up, on a sample holder. Some of the samples were metallized to ease charge elimination (20 nm of gold) and examined with two scanning electron microscopes (SEM). A low-resolution Philips XL20 was chosen for preliminary explorations and a JEOL 7500F high-resolution field-effect SEM was used for more detailed examinations. Non-metallized samples were examined under a “gentle beam” mode where electrons decelerate before touching the sample surface, avoiding charge build up.

SEM analysis is a two-dimensional surface analyzing technique: to be able to see the region of interest (ROI), this one has to be accessible to the electrons. That means, in the case of the firefly, we have to cut the lantern open to see the inside. **Nanotomography** in contrary is a three-dimensional analyzing technique, where the whole lantern can be scanned. Preparation of the samples included embedding in epoxy resin to stabilize spatially the sample. Other samples could be mounted immediately on the experimentation stage, without any preparation. The experiment has been carried out on the micro-imaging beamline *ID22* at the European Synchrotron Radiation Facility (ESRF). Holotomography has been used on our samples, i.e. quantitative phase tomography with a coherent hard synchrotron radiation x-ray beam [20]. Holotomography is used when the difference in density between components is weak, as in the firefly case. The sample is rotated 360° and two-dimensional projection images are taken at numerous angle positions. This procedure was repeated for three additional and well defined distances which leads to three-dimensional reconstructions.

Reflectivity and transmittivity spectra are calculated with **three-dimensional transfer-matrices** [13], a computational technique designed to describe the propagation of light in a photonic-crystal film from Maxwell’s equations. This technique produces the intensity, at a fixed frequency, of each forward or backward diffracted beam from an inhomogeneous dielectric film with a two-dimensional lateral periodicity surfaces. Note that in this approach, the refractive index is not averaged laterally over periodic planes, so that both the lateral and normal inhomogeneities are fully accounted for. Technically, the transfer-matrix approach uses the same basis as the RCWA (rigorous coupled-wave analysis) technique used for calculating the intensity of diffracted waves on gratings [21]. A one-dimensional, fully vector, version valid for a general planar multilayer, and a full three-dimensional version of this algorithm are available and used for the calculations needed in all simulations. The algorithm is highly stable for both one- and three-dimensional cases, thanks to the special way of constructiong the final scattering matrix, which relates all outgoing waves to given ingoing wave. In three-dimensional cases, the final scattering matrix results from the fine slicing of the structured film, the construction of the scattering matrix for each slice from the solution of Maxwell’s equation and the analytic assembly of all scattering matrices. The calculation is essentially exact, except for the limited number of terms in the Fourier representation of the periodic lateral parts of the fields and dielectric functions and a staircase assumption, which considers that the refractive index is constant in each fine slice in the normal direction.

The radiance measurements have been carried out on a **scatterometer EZ Contrast XL80MS** built by the French company ELDIM. This instrument is essentially a system of Fourier lenses that redirect all light rays emitted along all emergence directions in such a way that they form an image of the source on a plane (called the “Fourier plane”). Each direction, characterized by a polar angle and an azimuthal angle is mapped to a point on a disk on the Fourier plane. The image is then transferred to a CCD captor. While being transferred, the light is filtered in order to pass only a small range of wavelengths (about 10 nm of spectral width window). The captor measures all the intensities in the disk-shaped map which contains a planar projection of the intensity distribution in the emergence hemisphere. 31 colored filters, covering the visible region, allow to produce a complete relevant spectrum with a reasonable wavelength resolution. The result is the radiance (in units of $W/m^2/nm/sr$) finely analyzed angularly over a complete range (2π) of azimuthal angles and a nearly complete (from 0° to 80°) range of polar angles, for 31 wavelengths covering the visible spectrum. This instrument is used here to give a direct measurement of the the light scattered by the photocytes of a firefly illuminated by light brought into the firefly lantern, through an optical fiber (diameter 200 μm), from an external white source. The source used for internal illumination is 300W EZ Reflex Source lamp which is able to deliver a maximal luminous emittance of 3000 lx. The radiance was integrated over all emergence angles to produce an absolute value of the emitted power per unit surface and unit wavelength.

Acknowledgments

We thank Dr. Jean-François Colomer for his help in the scanning-electron microscopes operation. J.P.V. thanks Dr. Alan R. Gillogly, Curator of Entomology at the Orma J. Smith Natural History Museum, Caldwell, Idaho, USA, and Dr. Donald Windsor for help in collecting the specimens of fireflies used in the present study. Both authors acknowledge very helpful discussions with Prof. Helen Ghiradella (State University of New York, Albany, USA), Dr. Laure Bonnaud (Museum National d'Histoire Naturelle, Paris France), Prof. Laszlò Birò (Nanostructures Department MFA, Research Institute for Technical Physics and Materials Science MTA, Hungarian Academy of Sciences, Budapest), Dr. Jérôme Loicq (Liège Space Center, Belgium), Dr. Pol Limbourg (Royal Belgian Institute of Natural Sciences, Brussels, Belgium), Dr. Gary Hevel and Dr. Warren Steiner (National Museum of Natural History, Smithsonian Institution, Washington D.C., USA). The X-ray nanotomography experiment was carried out at the nano-imaging endstation ID22NI of the European Synchrotron Radiation Facility (ESRF) in Grenoble (France). A. B. was supported as PhD student by the Belgian Fund for Industrial and Agricultural Research (FRIA). The project was partly funded by the Action de Recherche Concertée (ARC) Grant No. 10/15-033 from the French Community of Belgium. The authors also acknowledge using resources from the Interuniversity Scientific Computing Facility located at the University of Namur, Belgium, which is supported by the F.R.S.-FNRS under convention No. 2.4617.07.

-
- [1] A. Vezzi, S. Campanaro, M. D'Angelo, F. Simonato, N. Vitulo, F. M. Lauro, A. Cestaro, G. Malacrida, B. Simionati, N. Cannata, C. Romualdi, D. H. Bartlett, and G. Valle, "Life at depth: *Photobacterium profundum* genome sequence and expression analysis," *Science* **307**(5714), 1459–1461 (2005).
 - [2] H. Ghiradella, "The anatomy of light production : The fine structure of the firefly lantern," In *Microscopic Anatomy of Invertebrates* **11A : Insecta** 363–381 (Wiley-Liss, 1998).
 - [3] R.F. Chapman, *The Insects. Structure and Function*. 4th edition, (Cambridge University Press, Cambridge UK, 1998).
 - [4] J.E. Lloyd, "Aggressive mimicry in *Photuris* : firefly femmes fatales," *Science* **149**, 653–654 (1965).
 - [5] T. Eisner, M. A. Goetz, D. E. Hill, S. R. Smedley, and J. Meinwald, "Firefly "femmes fatales" acquire defensive steroids (lucibufagins) from their firefly prey," *Proc. Natl. Acad. Sci. USA* **94**, 9723–9728 (1997).
 - [6] A. Bay, and J. P. Vigneron, "Light extraction from the bioluminescent organs of fireflies," *Proc. SPIE 7401 : Biomimetics and Bioinspiration* **740108**, 1–12 (2009).
 - [7] H. Benisty, "Physics of light extraction efficiency in planar microcavity light-emitting diodes," In *Lecture Notes in Physics: Confined Photon Systems* **531**, 393–405 (Springer, Berlin 1999).
 - [8] P. Vandersteegen, A. U. Nieto, C. Van Buggenhout, S. Verstuyft, P. Bienstman, P. Debackere, K. Neyts, and R. Baets, "Employing a 2D surface grating to improve light out coupling of a substrate emitting organic LED," *Proc. SPIE 6486: Light-Emitting Diodes: Research, Manufacturing, and Applications XI* **64860H**, DOI: 10.1117/12.701344 (2007).
 - [9] P. Vandersteegen, S. Mladenovski, V. Van Elsbergen, G. Gartner, P. Bienstman, K. Neyts, and R. Baets, "Light extraction for a doubly resonant cavity organic LED: the RC2LED," *Proc. SPIE 6655: Organic Light Emitting Materials and Devices XI* **665513**, DOI: 10.1117/12.732524 (2007).
 - [10] I. B. J. Sollas, "On the identification of chitin by its physical constants," *P. Roy. Soc. B - Biol. Sci.* **79** (534), 474–481 (1907).
 - [11] P. Vukusic, J.R. Sambles, C.R. Lawrence, and R.J. Wootton, "Quantified interference and diffraction in single *Morpho* butterfly scales," *P. Roy. Soc. B - Biol. Sci.* **266**, 1403–1411 (1999).
 - [12] S. Yoshioka, and S. Kinoshita, *Phys. Rev. E*, **83**, 051917 (2011).
 - [13] G. Forsythe, M. Malcolm, and C. Moler, *Computer Methods for Mathematical Computations*, (Prentice-Hall, Englewood Cliffs, NJ 1977).
 - [14] C. de Duve, "The peroxisome: a new cytoplasmic organelle," *P. Roy. Soc. B - Biol. Sci.* **173** (30), 71–83 (1969).
 - [15] P. Vukusic, and I. Hooper, "Directionally controlled fluorescence emission in butterflies," *Science* **310**(5751), 1151 (2005).
 - [16] J.P. Vigneron, and V. Lousse, "Variation of a photonic crystal color with the Miller indices of the exposed surface," *Proc. SPIE conference 6128: Photonic Crystal Materials and Devices IV* **6128**, 1G 1–10 (2006).
 - [17] V. Lousse, J.-P. Vigneron, X. Bouju, and J.-M. Vigoureux, "Atomic radiation rates in photonic crystals," *Phys. Rev. B* **64**(20), 201104(R) (2001).
 - [18] L. De Vico, Y.-J. Liu, and R. Lindh, "Ab initio investigation on the chemical origin of the firefly bioluminescence," *J. Photoch. Photobio. A* **194**, 261–267 (2008).
 - [19] J.P. Vigneron, J.-F. Colomer, N. Vigneron, and V. Lousse, "Natural layer-by-layer photonic structure in the squamae of *Hoplia coerulea* (Coleoptera)," *Phys. Rev. E* **72**, 061904 (2005).
 - [20] P. Cloetens, W. Ludwig, J. Baruchel, D. Van Dyck, J. Van Landuyt, J. P. Guigay, and M. Schlenker, "Holotomography: Quantitative phase tomography with micrometer resolution using hard synchrotron x rays," *Appl. Phys. Lett.* **75** (19), 2912–2914 (1999)
 - [21] M. G. Moharam, and T. K. Gaylord, "Rigorous coupled-wave analysis of planar-grating diffraction," *J. Opt. Soc. Am.* **71**, 811–818 (1981)